

## Supplemental Material

### Magnetism and Thermal Transport of Exchange-Spring-Coupled $\text{La}_{2/3}\text{Sr}_{1/3}\text{MnO}_3/\text{La}_2\text{MnCoO}_6$ Superlattices with Perpendicular Magnetic Anisotropy

Vitaly Bruchmann-Bamberg<sup>1</sup>, Isabell Weimer<sup>1</sup>, Vladimir Roddatis<sup>2</sup>, Ulrich Ross<sup>3</sup>, Leonard Schüler<sup>1</sup>, Karen P. Stroh<sup>1</sup>, Vasily Moshnyaga<sup>1</sup>

<sup>1</sup>*Erstes Physikalisches Institut, Georg-August-University Göttingen, Friedrich-Hund-Platz 1, 37077 Göttingen, Germany*

<sup>2</sup>*Helmholtz Centre Potsdam, GFZ German Research Centre for Geosciences, Telegrafenberg, 14473 Potsdam, Germany*

<sup>3</sup>*IV. Physikalisches Institut, Georg-August-University Göttingen, Friedrich-Hund-Platz 1, 37077 Göttingen, Germany*

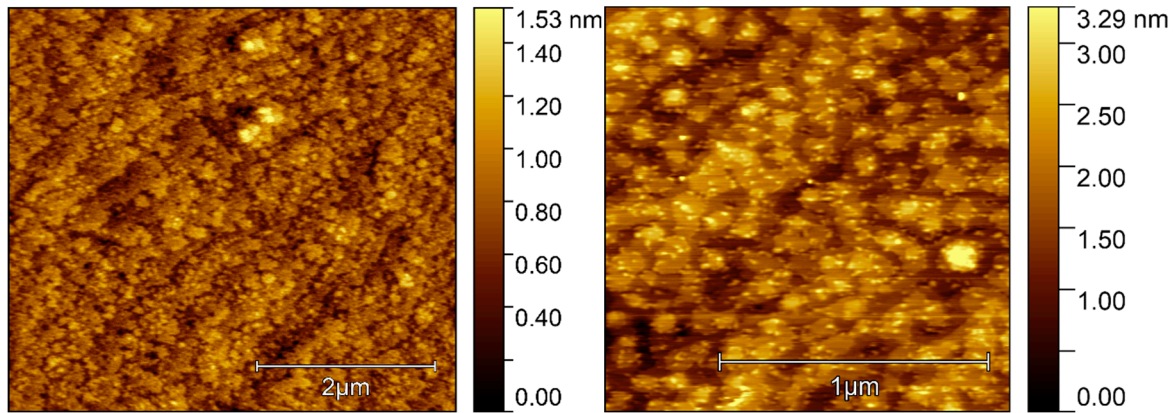


**Figure S1** Left: Atomic force microscope topography of the  $[(\text{LMCO})_n/(\text{LSMO}_n)]_m/\text{STO}(100)$  n=9 u.c. SL (RMS roughness  $S_q=0.2(1)$  nm); Right: SL n=24 u.c. ( $S_q=0.5(1)$  nm)

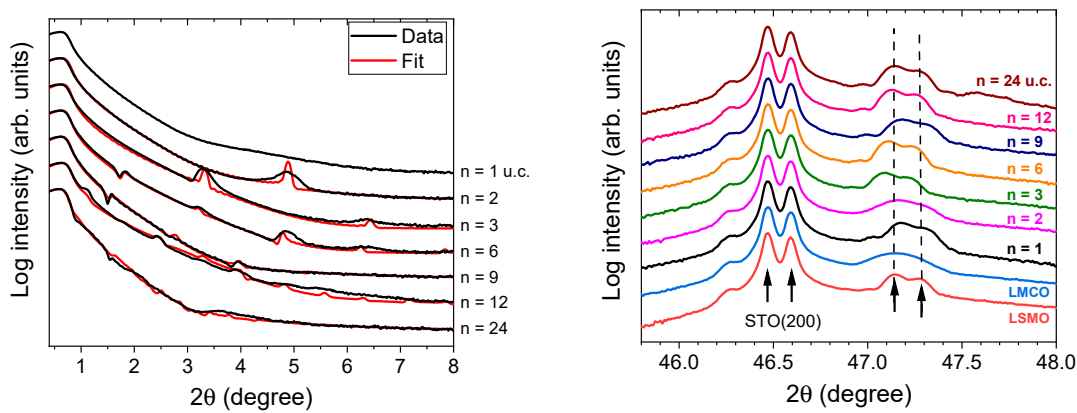


**Figure S2** Left: XRR patterns (black curves) and fitting curves using the program GenX 3 [40] of  $[\text{LSMO}_n/\text{LMCO}_n]_m/\text{STO}(100)$  SLs revealing superstructure peaks of the bilayers. The fit parameters are listed in Table S1. Right: X-Ray diffraction patterns of the SLs reveal a very similar out-of-plane lattice parameter  $c \approx 3.852 \pm 0.004$  Å for all SLs and single LSMO and LMCO films. The arrows indicate the  $k_{\alpha 1}/k_{\alpha 2}$  splitting of the STO(200) peak and of the (002) peak of most SLs.

[40] A. Glavic and M. Björck, “GenX 3: the latest generation of an established tool”, J. Appl. Cryst. 55, 1063 (2022)

**Table S1** GenX 3 fit parameters for  $[\text{LSMO}_n/\text{LMCO}_n]_m/\text{STO}(100)$  SLs

n (u.c.)	Targeted bilayer thickness $d_{2n}$ (nm)	Measured $d_{2n}$ (nm)	Deviation per bilayer	Average interfacial roughness $\sigma_{\text{RMS}}$ (nm)
2	1.54	1.85	+ 1 u.c.	0.4
3	2.31	2.75	+ 1 u.c.	0.5
6	4.62	5.68	+ 3 u.c.	0.5
9	6.93	7.06	< 1 u.c.	0.9
12	9.24	11.5	+ 6 u.c.	0.6
24	18.49	21.1	+ 7 u.c.	1.1

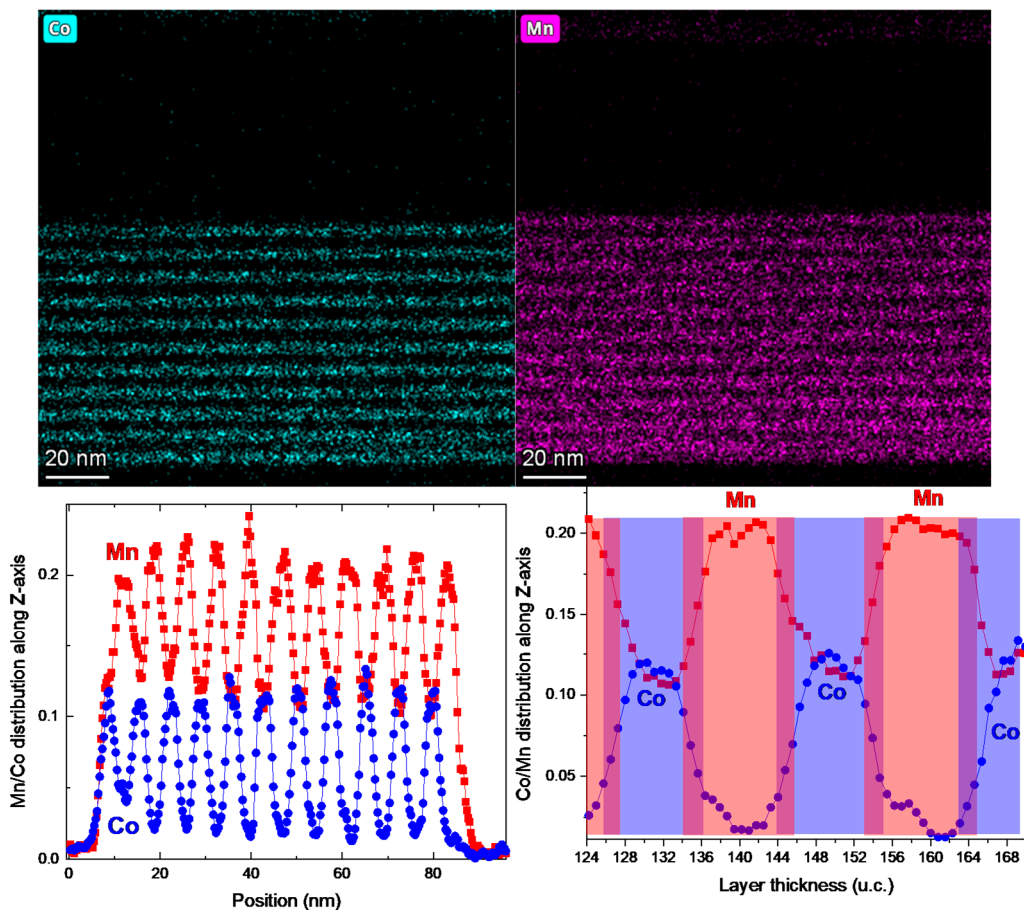


**Figure S3** Distribution of Co (top, left) and Mn (top, right) atoms within the  $[(\text{LMCO})_9(\text{LSMO})_9]_{11}$  SL obtained by using energy dispersive X-ray microanalysis (EDX) (left panels) shows a clear chemical contrast between the LMCO and the LSMO layers. A linear scan along the growth direction of the whole SL (bottom, left) and along the selected layers in the middle of SL (bottom, right), from which a (Co/Mn) intermixing at the LSMO/LMCO interfaces with a thickness  $\sim 2$  u.c. can be deduced.

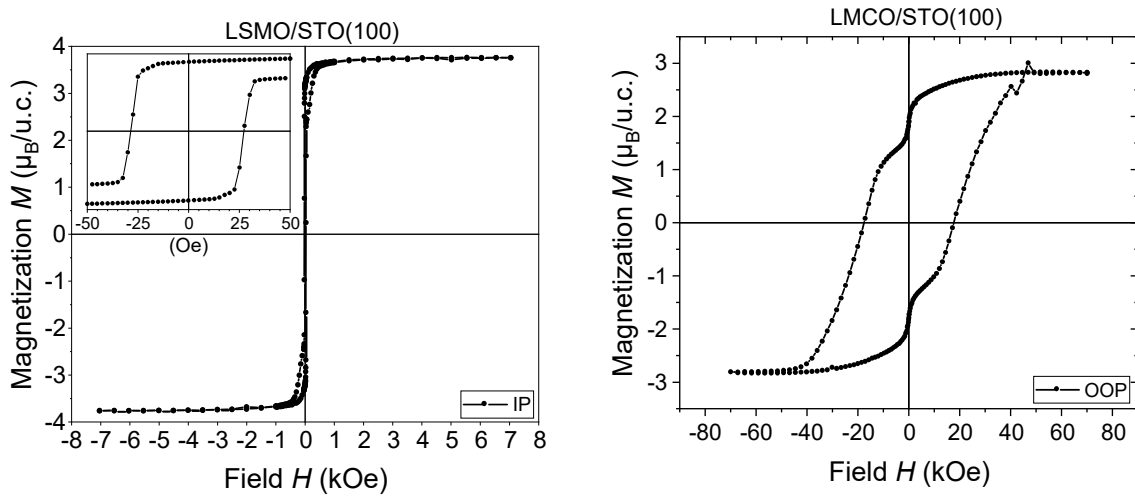


**Figure S4:** Magnetic hysteresis loops for LSMO/STO(100) (left) and LMCO/STO(100) (right) at 5K along their respective easy axis.

**Table S2:** Saturation magnetization and coercive field of LSMO/STO(100) and LMCO/STO(100) along their easy axis.

	$M_{\text{sat}}$ [ $\mu_B/\text{u.c.}$ ]	$H_c$ [Oe]
LSMO/STO(100) IP	3.8(1) (theory: 3.7)	30(10)
LMCO/STO(100) OOP	2.8(1) (theory: 3)	17600(100)

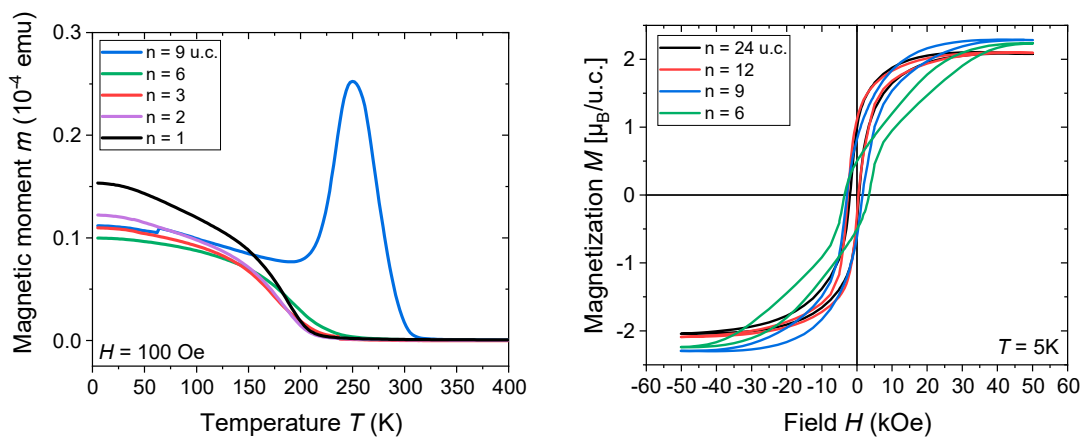


**Figure S5** Left: Field-cooled IP magnetic moment of the  $[(\text{LMCO})_n/(\text{LSMO}_n)]_m/\text{STO}(100)$  ( $n = 1-9$  u.c.) superlattices at low magnetic field. Spin reorientation transition is missing in SLs with very thin LSMO and LMCO layers. Right: IP Magnetic hysteresis loops of selected  $[(\text{LMCO})_n/(\text{LSMO}_n)]_m/\text{STO}(100)$  superlattices.

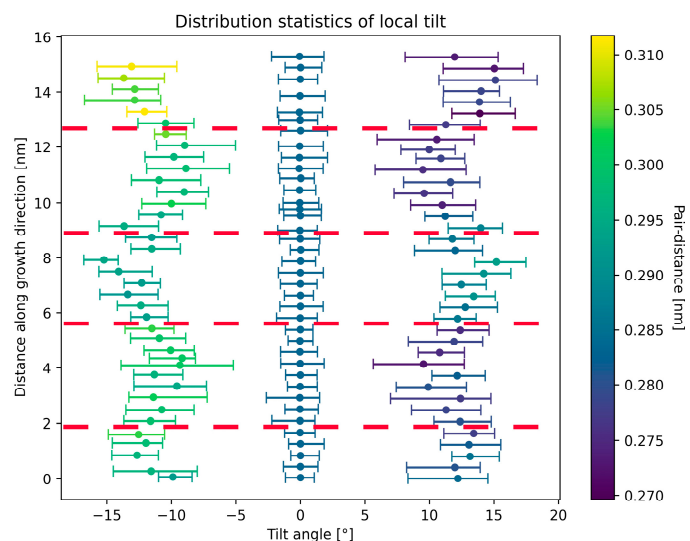
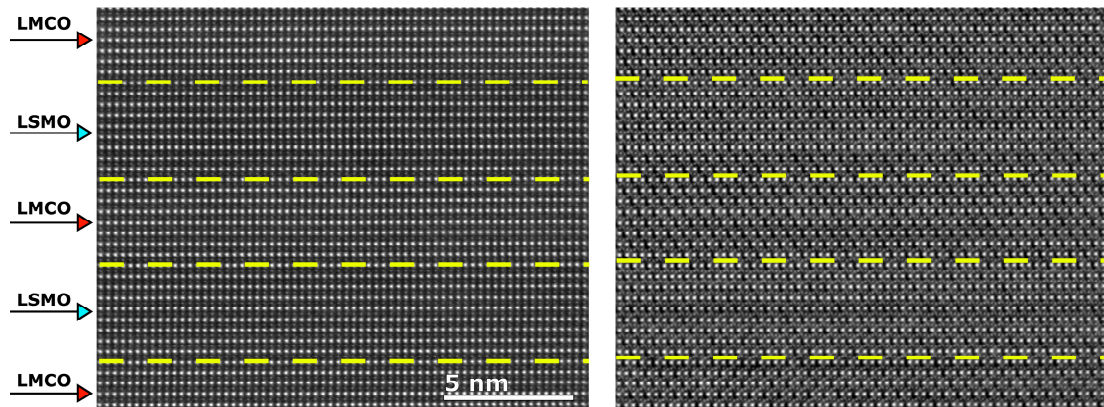


**Figure S6** ADF-STEM (top, left), iDPC (top, right) images of the  $[LSMO_9/LMCO_9]_{11}/\text{STO}(100)$  superlattice, with the corresponding evaluation of octahedral tilt angles  $\theta$  within the image plane (bottom). Connection to the Mn-O-Mn(Co) angle in the main text is done via  $\varphi_{B-O-B} = 180^\circ - 2\theta$ . The central cluster around  $\theta = 0^\circ$  (on the right panel) corresponds to the Mn-Mn pairs, while the datapoints around  $\theta = \pm 12^\circ$  correspond to the Mn-O-Mn(Co) bond chains. The analysis reveals continuous change of the octahedral tilt angle at the interfaces between LMCO ( $\theta_{\text{LMCO}} \approx 13^\circ$ ) and LSMO ( $\theta_{\text{LSMO}} \approx 10^\circ$ ). Error bars indicate the maximum scattering of the angles within one layer, while the standard deviation for all layers lies in the range of  $\sigma(\theta) = 0.5\text{--}1.5^\circ$ .

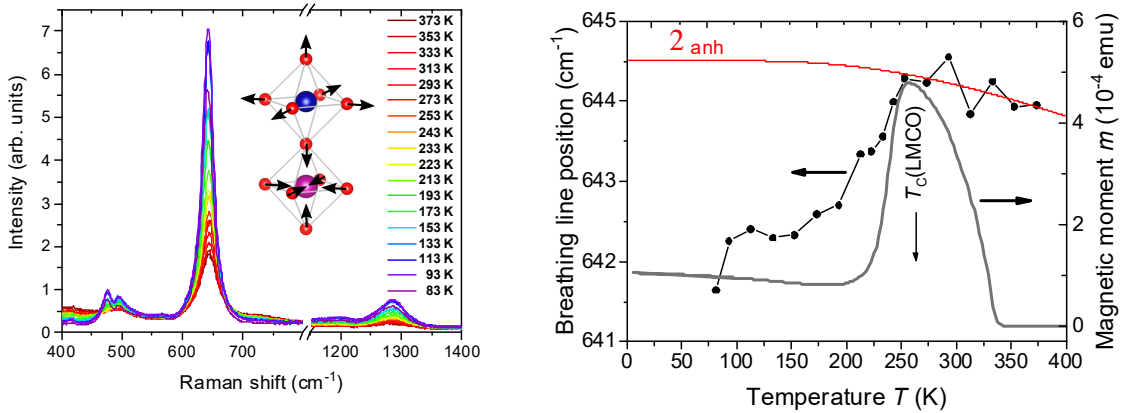


**Figure S7** Left: Raman spectra of the  $n = 24$  u.c. SL  $[(\text{LSMO})_{24}/(\text{LMCO})_{24}]_4/\text{STO}(100)$  measured for different temperatures in the range  $T \approx 100\text{-}400$  K and an illustration of the  $644 \text{ cm}^{-1}$  breathing mode vibration; Right: Temperature dependence of the position of the breathing line (left scale) and IP magnetic moment (right scale) indicates a significant increase of the Curie temperature of the LMCO layers within the SL up to about  $T_{c,\text{LMCO}} \approx 260$  K. The red line is a fit to the anharmonic line shift  $\omega(T) = \omega_0 + C(1 + 2/(e^{\hbar\omega_0/2k_B T} - 1))$  [67] for temperatures  $T > T_{c,\text{LMCO}}$ .

[67] Balkanski, M., Wallis, R. F. & Haro, E. Anharmonic effects in light scattering due to optical phonons in silicon. *Phys. Rev. B* **28**, 1928 (1983).

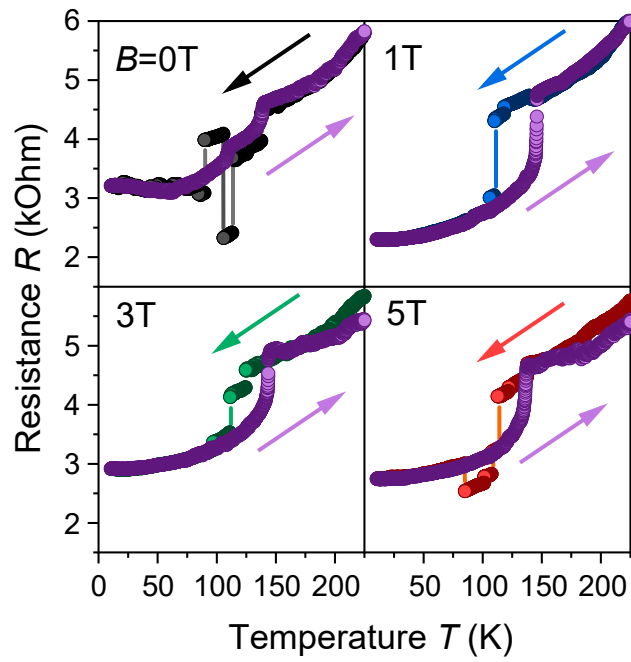


**Figure S8** Electrical resistance vs temperature (both current and magnetic field applied in-plane) in the vicinity of structural phase transition in STO at  $T^* = 105$  K for the  $[(\text{LMCO})_9/(\text{LSMO}_9)]_{11}/\text{STO}(100)$  SL at different magnetic fields. The arrows indicate the direction of the temperature scan.

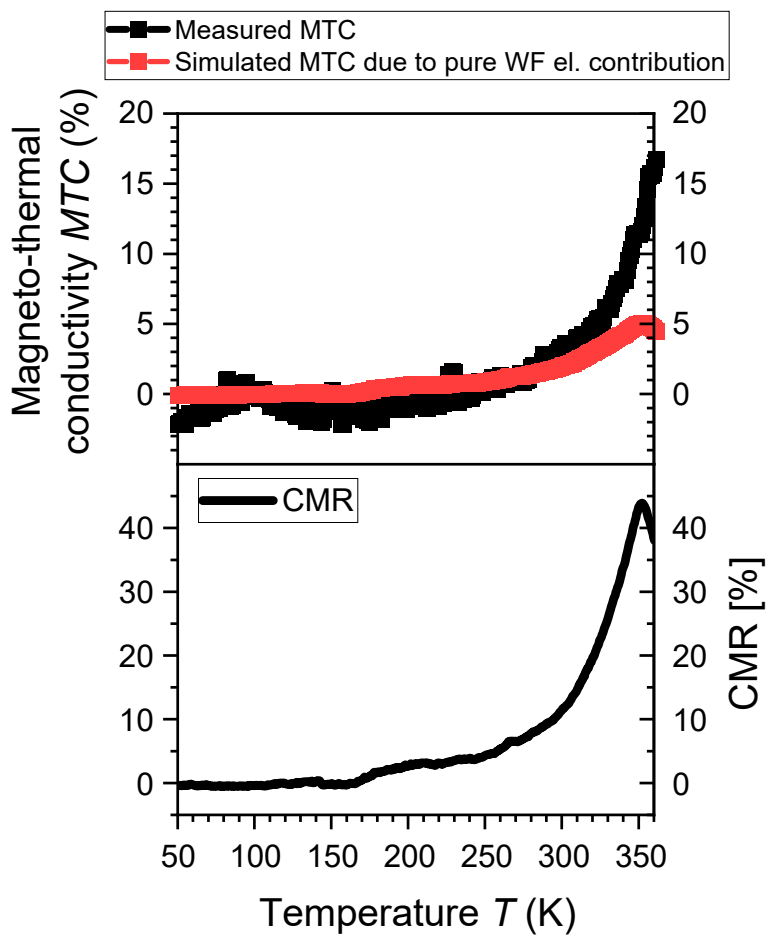


**Figure S9** Top panel: measured magneto-thermal conductivity,  $MTC=100\% * [\kappa(5 T) - \kappa(0)] / \kappa(0)$ , (black points) and the estimated from the Wiedemann-Franz (WF) law for electronic contribution to MTC due to CMR (red points) of the single LSMO/STO(100). Bottom panel: colossal magnetoresistance  $CMR=100\% * [R(0) - R(5 T)] / R(0)$  of the LSMO/STO(100) thin film shows a typical behaviour with a peak close to  $T_c \approx 350$  K.